Instability problem of the electric field antennas on the Polar spacecraft

E. Kolesnikova, Christian Béghin

Radio Science, Volume 36, Number 2, Pages 203–221, March/April 2001

Instability problem of the electric field antennas on the Polar spacecraft

E. Kolesnikova[1] and C. Béghin

Laboratoire de Physique et Chimie de l'Environnement, Centre National de la Recherche Scientifique Orléans, France

Abstract. This paper is an application of the surface charge distribution method to the modeling of the electric antennas installed on board the Polar spacecraft in order to identify the plasma conditions leading to the instability of the sphere-preamplifier-stub-guard system. First we present an analytic approach, which allows us to understand the physical mechanism and to define the conditions of the instability. We then show the results of the numerical modeling for the more common types of instabilities observed in flight. The latter, which we call type-1 oscillations, are observed solely in the low-L plasmasphere region. The modeling predicts that the oscillations can occur in a weakly magnetized Maxwellian plasma in the upper hybrid range ($f_p < f < f_t$) when the Debye length lies between well-defined limits. The frequency modulation of the oscillations in this range versus the spin angle of the antennas with respect to the Earth's magnetic field is well explained by the model. The type-2 oscillations are observed occasionally and occur always in the exterior cusp, at large L values. They are most likely to be associated with high-density clouds of solar wind streaming plasma entering into that region. Our analytic modeling indeed predicts that the instability conditions can be satisfied when the antennas are crossing a 10 eV electron flow, with a density of ~100 cm^{-3} and a bulk velocity of the order of 200 km s^{-1}.

1. Introduction

The Polar satellite, designed for studying the Earth's magnetosphere, was launched on February 24, 1996. A few months after the launch, the principal investigators of Polar's Electric Field Instrument (EFI) [*Harvey et al.*, 1995] and Plasma Wave Instrument (PWI) [*Gurnett et al.*, 1995] informed their coinvestigators that the two electric field antennas E_u and E_v perpendicular to the spin axis had a tendency to oscillate in particular conditions, mainly in high-density plasma. The oscillations were unambiguously attributed to the electronic bootstrap system controlling the ac voltage of each pair of guard stubs surrounding the spherical sensors installed at the tips of four perpendicular wire booms.

The frequency spectrum of the oscillations is characterized by a main line assumed to lie near the plasma frequency, and occasionally several harmonics of this line and a broadband low-frequency noise probably generated by saturation of the electronics are also seen. This instability was observed nearly every orbit as Polar passed through the plasmasphere, at low L shell values (D. A. Gurnett and J. Pickett, unpublished memorandum, 1996). In addition, some rare cases have been identified in the magnetosphere at a distance of 7-9 Earth radii. In the first case, the frequency of the oscillations lies between 150 and 400 kHz, whereas in the second case the frequency remains confined to a fairly narrow range below the previous one, extending from 70 to 110 kHz. The analyzed data do not reveal any oscillation of the on-axis short-dipole antenna E_z by itself. However, the instability of the other two antennas, which is observed on E_z, and even on magnetic search coils, is interpreted as a mutual induction of the oscillation frequency through the plasma.

[1] Now at Department of Physics and Astronomy, University of Leicester, England, United Kingdom.

Paper number 1999RS002303.
0048-6604/01/1999RS002303$11.00

Since a passive antenna system must be stable in any plasma conditions; the instability comes indeed from the active part of the antenna design. Each half-dipole antenna on the Polar satellite [*Harvey et al.*, 1995] is made of a spherical sensor with nearby stubs whose potential relative to that of the sphere is controlled by feedback from the preamplifier output such that those stubs are used as electric guards. This construction was designed to control the flow of photoelectrons between the spheres and the other parts of the boom during the measurements in the dc and very low frequency ranges. Unfortunately, such an active device is known to become unstable at higher frequency under certain conditions [*Fiala,* 1970], though there are no more reports of this in the literature to date.

In order to check this initial presumption the impedance of such a double-sphere dipole has been computed using the surface charge distribution (SCD) method [*Béghin and Kolesnikova,* 1998] with a forced following voltage applied on the stubs. The result confirmed that in the vicinity of the plasma frequency a negative value of the dipole resistance appears for certain values of the Debye length [*Béghin and Kolesnikova*, 1997]. This is due to mutual coupling between the spherical sensor and the stubs through the plasma, whose strength with respect to free-space conditions increases considerably to produce the feedback instability.

We develop here a different approach, based on the Nyquist criterion applied to the open-loop transfer function between the guard-stubs and the spherical sensor, allowing us to perform a preliminary analytic evaluation before commencing numerical modeling. In order to account for observations of oscillations in different geophysical situations and to explain their particular features, we will consider three different plasma models, i.e., first, an ideal steady and purely isotropic Maxwellian distribution, second, a weakly magnetized plasma, such that the plasma frequency is significantly larger than the electron gyrofrequency ($f_p > 3f_c$), and, finally, a streaming plasma with a ratio of bulk over thermal velocities of the order of 10%.

We present first an analytic demonstration of the instability conditions for the general case, which leads to the evaluation of the critical plasma parameters for each plasma model which we considered. We will then compare these results with those of the numerical modeling using the SCD method in a quasi-isotropic and steady plasma. While the predicted plasma parameters satisfying the instability conditions are found to be consistent with typical geophysical values in the plasmasphere region, where type-1 oscillations are observed, these parameters are not realistic for the oscillations occurring at large L values in the outer cusp region (type 2). In the latter case, a simplified analytic approach will show that a relatively weak bulk velocity of the plasma may significantly modify the critical parameters up to values compatible with those reasonably expected in the considered region.

2. Observations of Instabilities

The Polar's EFI antenna array [*Harvey et al.*, 1995] consists of two sphere pairs (E_u and E_v) mounted at the ends of wire booms, with a tip-to-tip sphere separation of 130 and 100 m, respectively, located in the satellite spin plane, and also a third pair (E_z), aligned along the spacecraft spin axis with a 13.8 m tip-to-tip separation (Figure 1). Each sphere of 8 cm diameter encloses a built-in preamplifier. Basically, the spherical sensors are taking an ac voltage V_s resulting from the balance between the input current of the preamplifier and the current flowing out in the plasma, which is the current induced by any external ac electric field. In addition, the spheres are electrically insulated over a distance of 3 m (for E_u-E_v) or 64.6 cm (for E_z) from the screened wire boom through a voltage follower stub. An identical stub is mounted in the opposite direction to the previous one. The ac follower voltage on the stub surfaces V_b is controlled by the preamplifier output through a capacitance C_s [*Harvey et al.*, 1995, Figure 4]. A simplified equivalent scheme of the system and the high-frequency transfer function of the preamplifier, as used in our modeling, are given in Figures 2 and 3, respectively.

The best way to unambiguously characterize the instability phenomenon is by a comparison of both PWI and EFI selected data [J. Pickett, University of Iowa, private communication, 1997; *Escoubet et al.*, 1997], which allows us to identify the instability periods and the sensor which is oscillating. The PWI wide band spectrograms show the spectral characteristics of the oscillations superposed to natural signals, while the preamplifiers of the spheres drop to dc saturation when the instability occurs (Plate 1). Such a data analysis also shows that the current induced by the oscillations of a given sensor is strong enough to be seen by the other antennas, even by the magnetic coils.

We will consider here, as a case study, a portion of the orbit of May 11, 1997, shown in Plate 1. At this time the oscillations are observed on the antenna E_u and they occur during two different sequences. The

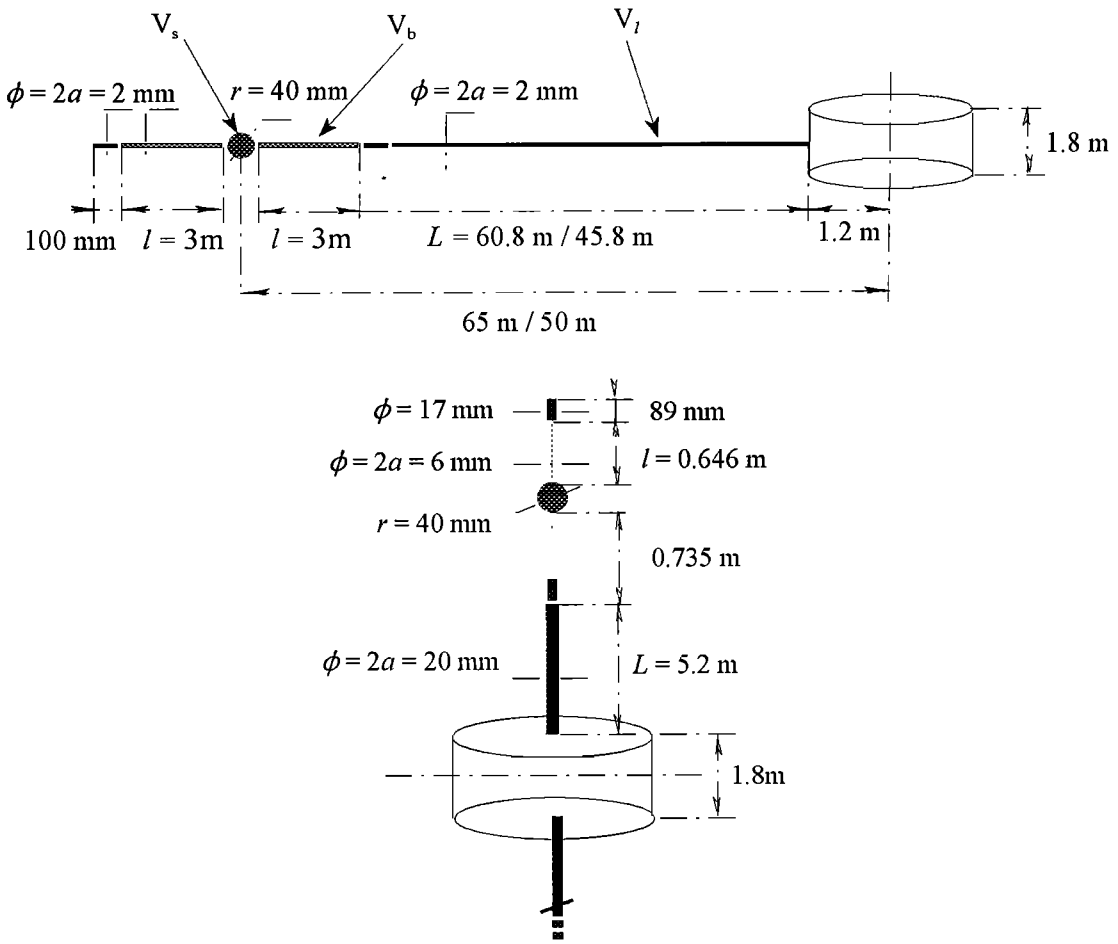

Figure 1. Schematic drawing of the Polar electric antennas, (top) E_u-E_v and (bottom) E_z.

first one appears between 0100 and 0500 spacecraft event time (SCET), in the apogee region beyond 8 Earth radii and at L values larger than 20. On the PWI wide band spectrogram of the E_u antenna the oscillation lies between 70 and 110 kHz, and the harmonic lines produced by the preamplifier saturation are visible up to 500 kHz. The plots of quasi-dc voltages of one sensor of each antenna E_u and E_z exhibit clearly the disturbance of the E_u preamplifier while that of E_z is not disturbed.

The second sequence is seen almost 7 hours later, just before 1200 SCET, in the perigee region at ~3 Earth radii, in the low-latitude conventional plasmasphere (L ~ 3). Here the oscillation frequency

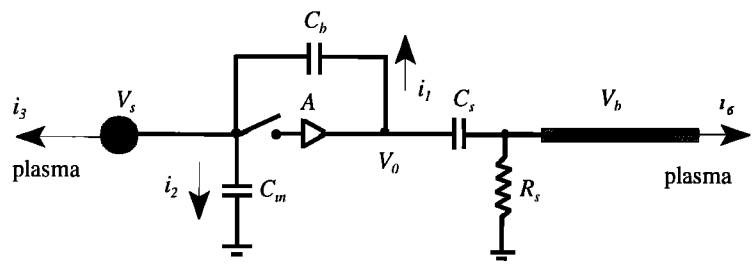

Figure 2. Equivalent electric scheme of the sphere-stub coupling in open-loop configuration.

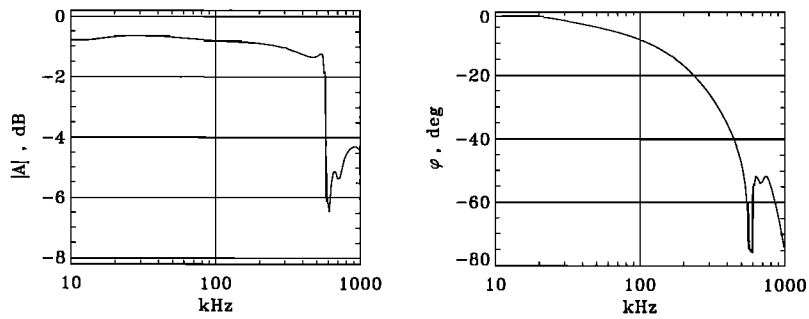

Figure 3. Transfer function of the preamplifier above 10kHz, after L. Åhlen (private communication, 1997).

is significantly higher than in the previous sequence (200-300 kHz), but the features of the preamplifier saturation are the same. Since the beginning of the mission this phenomenon has been frequently observed in the low-latitude perigee region, and the oscillation frequency was soon expected to lie near the local plasma frequency (D. A. Gurnett and J. Pickett, unpublished memorendum, 1996). On the contrary, the occurrence of oscillations in the high-altitude and high-latitude region of the first sequence in Plate 1 is rather unusual. Apart from those two well-characterized regions, instabilities have never been observed elsewhere along the Polar orbit.

In the following, we call type-1 instabilities those occurring frequently at low altitude as during the second sequence in Plate 1, and type 2 those observed at large distance outside the polar cusp. There are, to date, only five well-identified type-2 events, though a systematic investigation could reveal more examples. For all five events the oscillation frequency lies in the range 70-110 kHz, i.e., at least 2 times lower than the usual range of type-1 oscillations. The duration of type-2 instabilities is extremely variable, from less than 2 min up to more than 3 hours, and they appear often as broken events, in contrast to type-1 instabilities, which are always occurring in a regular medium.

For the case of the type-1 events a telemetry mode for high-time-resolution spectrograms which was occasionally used allows us to emphasize the evolution of the oscillation during the spin period. One example of this mode is shown as a short portion of the perigee pass on April 8, 1996, in Figure 4. The simultaneous plotting of the magnetometer data shows, first, that the oscillations observed on a given dipole are frequency and amplitude modulated at twice the spin period. The variations of the oscillation frequency during one period never exceed the estimated difference between the local plasma frequency and the upper hybrid resonance. Moreover, the plots in Figure 4 clearly show that the higher frequency is observed while the angle between the dipole and the Earth's magnetic field $\mathbf{B}_0$ is minimum and the lower frequency is observed when the dipole is perpendicular to $\mathbf{B}_0$. When the instability is at the point of vanishing (after 1203 SCET), the oscillation occurs only when the dipole becomes aligned with $\mathbf{B}_0$.

Unfortunately, the fine structure of type-2 oscillations is much more difficult to determine for two reasons; one is due to the turbulent character of the phenomenon, and the second is due to its low occurrence. This point will be the subject of a further analysis, and we will retain here only that the dc voltage of individual sensors during type-2 oscillations reveals a modulation at the spin period, contrary to type-1 oscillations, as the proof of an additional vectorial sensitivity in some orientation which is not that of magnetic field lines. The main characteristics of both types of oscillations and of expected plasma conditions in the regions where they occur are given in Table 1.

These remarkable features indicate that the instability conditions must be different for each type and must also be extremely selective with regard to the rarity of the type-2 events. For that reason, we will consider in section 3 different models of plasma which will be used in our theoretical investigation.

3. Description of Plasma

The SCD method makes use of the solution of Poisson's equation for the quasi-static potential induced in a plasma, at a given distance from a pulsating point charge [*Béghin and Kolesnikova,* 1998]. Initially, this method has been developed for an isotropic Maxwellian plasma. As a first-order approxi-

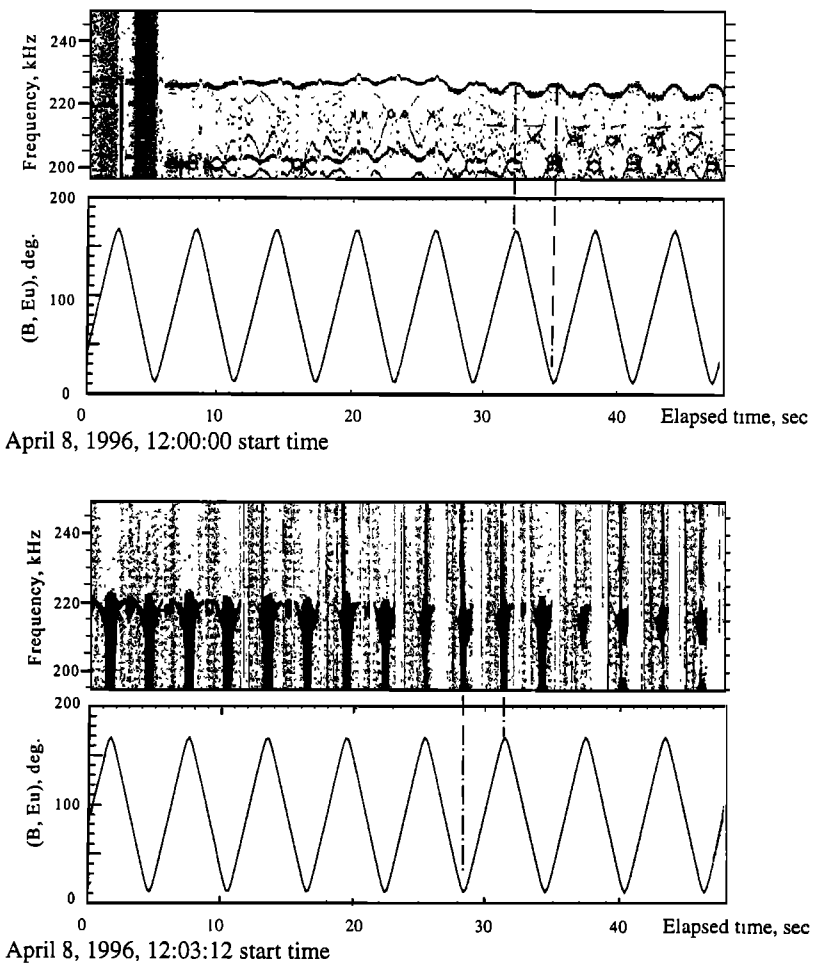

Figure 4. Silmultaneous plots of high-time resolution spectrogram of E_u's antenna oscillations and of the angle (E_u, $\mathbf{B}_0$) for the type-1 instability observed at the perigee pass on April 8, 1996, during two different time sequences around 1200 SCET (with permission of PWI experimenters D. Gurnett and J. Pickett).

mation, we will apply this approach to explain the mechanism of type-1 instability. However, in order to explain the fine structure of the antenna's oscillations we will use the solution given by the hydrodynamic approximation [*Kolesnikova and Béghin*, 1999a] in a weakly magnetized plasma ($f_p / f_c \geq 3$).

For the type-2 instabilities, occurring in the exterior cusp at 7-9 R_E, it is necessary to consider a more complicated description of the plasma by adding a bulk velocity, which is likely to be present in that region. We present in sections 3.1-3.3 an overview of the plasma dispersion characteristics and of the solution to Poisson's equation for each of the aforementioned plasma models.

3.1. Isotropic Thermal Plasma

The electrostatic dispersion relation, evaluated from the kinetic theory for an isotropic Maxwellian plasma, is written quite simply as

$$K_L(K,\Omega) = 1 - \frac{z^2}{\Omega^2} Z'(z), \qquad (1)$$

where K_L is the longitudinal dielectric constant and $Z'(z)$ is the first derivative of the dispersion function for the complex variable $z = \Omega/\sqrt{2}K$. We use here the dimensionless wave vector and frequency defined as $K = k\lambda_D$ and $\Omega = \omega/\omega_p$, respectively. The Debye length is defined as $\lambda_D = (\kappa T_e / m_e)^{1/2}/\omega_p$, with the

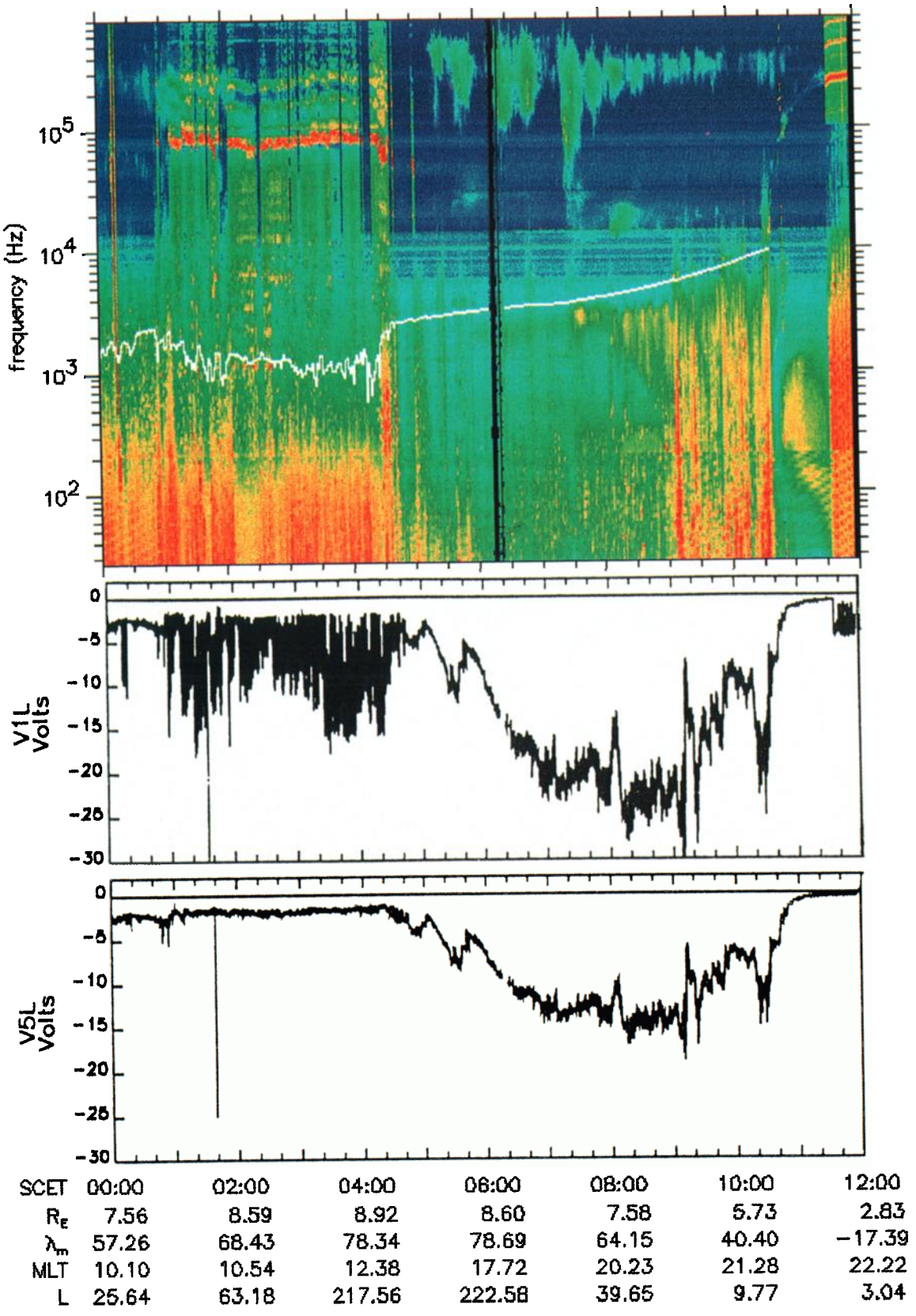
frequency (Hz)
10^5
10^4
10^3
10^2
V1L Volts
0
-5
-10
-15
-20
-25
-30
V5L Volts
0
-5
-10
-15
-20
-25
-30
SCET 00:00 02:00 04:00 06:00 08:00 10:00 12:00
R_E 7.56 8.59 8.92 8.60 7.58 5.73 2.83
λ_m 57.26 68.43 78.34 78.69 64.15 40.40 −17.39
MLT 10.10 10.54 12.38 17.72 20.23 21.28 22.22
L 25.64 63.18 217.56 222.58 39.65 9.77 3.04

Boltzmann constant κ. The dispersion characteristics of the longitudinal waves are mainly defined by a dominant pole, commonly known as a Landau wave, which is the solution of (1) using the approximation for $z \to \infty$. However, the full solution of (1) reveals in reality the existence of an infinity of poles which significantly contribute all together, at short distances from the source and at frequencies below ω_p, in the form of an electrokinetic mode [*Béghin,* 1995].

The solution of Poisson's equation for a pulsating point charge q exp ($i\omega t$), after Fourier-Laplace transforms, can be expressed as

$$V(\rho,t,\Omega) = \frac{q e^{i\omega t}}{(2\pi)^3 \varepsilon_0 \lambda_D} \iiint \frac{e^{-\imath \boldsymbol{K}\cdot\boldsymbol{\rho}} d^3K}{|K|^2 K_L(\boldsymbol{K},\Omega)}, \quad (2)$$

where ρ is the distance from the source, normalized to the Debye length.

In the vicinity of the plasma frequency the Landau wave approximation leads to a good estimation of (2), except for the imaginary part when Ω < 1 [*Béghin,* 1995]. In the analytic developments for isotropic plasma we will use this approximation, written as follows:

$$\begin{aligned} V_r &\approx \frac{q}{4\pi\varepsilon_o \lambda_D} \frac{1}{\rho \varepsilon_c} \left[1 - \frac{\exp(-i\rho\Omega\sqrt{\varepsilon_c/3})}{\Omega^2}\right] \\ &= \frac{q}{4\pi\varepsilon_o \lambda_D} U(\Omega,\rho) \qquad (3) \\ \varepsilon_c &= 1-\Omega^{-2},\ \rho = \frac{r}{\lambda_D},\ \mathrm{Im}(\Omega) \le 0, \end{aligned}$$

where the term exp (iωt) is now included in the charge q as an initial phase reference and $U(\Omega,\rho)$ is known hereafter as the plasma response.

At small distances, and near Ω = 1, this expression can be simplified again as

$$\begin{aligned} \mathrm{Re}\, U &\approx \frac{1}{\rho} - \frac{\delta}{\sqrt{3|\varepsilon_c|}} + \frac{\rho}{6} \\ \mathrm{Im}\, U &\approx (1-\delta)\left[\frac{1}{\sqrt{3|\varepsilon_c|}} - \frac{\rho^2\sqrt{|\varepsilon_c|}}{18\sqrt{3}}\right] \qquad (4) \end{aligned}$$

$\delta = 1$ for $\Omega < 1$, $\delta = 0$ for $\Omega \ge 1$, $\rho\sqrt{|\varepsilon_c|} \ll 3\sqrt{2}$.

In Figure 5 we show the behavior of the potential versus the distance from the source for two frequencies ±3% apart from the plasma frequency, as obtained with the full dispersion equation [*Béghin,* 1995]. The additional contribution of the electrokinetic mode in the form of a weak amplitude plateau is visible here in the imaginary part for Ω = 0.97 and ρ < 10.

It is important to emphasize here the different behavior of the plasma response between short and large distances at frequencies lower than the plasma frequency. One of the most important differences, which will be shown as the key for the instability mechanism, is the sign shift of the real part in the Debye region (ρ < 1) when Ω < 1 due to the balance between the free-space contribution, term 1/ρ in (4), and that of the plasma.

3.2. Weakly Magnetized Maxwellian Plasma

The dispersion equation of the longitudinal waves in a weakly magnetized warm plasma with $\omega_p/\omega_c \ge 3$, using a hydrodynamic description of the plasma [*Spitzer,* 1962; *Quemada,* 1968], can be reduced to the following approximation:

$$\begin{aligned} K_L &= \frac{\lambda_L^2}{\Omega_c^2 |K|^2}\left[\Omega_c^2 - \Omega_p^2 - \frac{\Omega_p^2}{\Omega_c^2 - 1}\sin^2\theta - 3K^2\right] = 0 \qquad (5) \\ \Omega_p &= \frac{\omega_p}{\omega_c},\ \Omega_c = \frac{\omega}{\omega_c},\ K = k\lambda_L, \end{aligned}$$

where θ is the angle between the **k** vector and the magnetic field vector $\mathbf{B}_0$. In the range of the upper hybrid frequencies, i.e., $\omega_p \le \omega \le \omega_t$, the real solutions of (5) can be written in the form

$$\begin{aligned} K &= \pm \frac{\Omega_p}{\sqrt{3(\Omega_c^2 - 1)}} \sqrt{\sin^2\theta_0 - \sin^2\theta} \qquad (6) \\ \sin\theta_0 &= \sqrt{(\Omega^2 - 1)(\Omega_c^2 - 1)},\ \Omega = \frac{\omega}{\omega_p} = \frac{\Omega_c}{\Omega_p}, \end{aligned}$$

Plate 1. Power spectrogram of the dipole E_u's signals and plots of the dc voltage of one of the E_u sensors (V1) and one of E_z sensors (V5), from the apogee region (0000 to 0800 SCET) to the perigee (1300 SCET), on May 11, 1997. The power scale ranges from red (10^{-8} V m^{-2} Hz^{-1}) down to violet (10^{-18} V m^{-2} Hz^{-1}), and the white curve is a superimposed plot of f_c; with permission of PWI and EFI experimenters D. Gurnett, J. Pickett, and F. Mozer.

Table 1. Summary of the Main Characteristics of Type-1 (Typical Case) and Type-2 (Identified Events) Instabilities

Type	Date	Duration	R_E	L	Expected Standard Plasma Parameters	Instability Frequency f_t, kHz	f_t/f_{ce}
1	-	~1hour event	~3	~3	n_e ~ 10-1000 cm^{-3} T_e ~ 1 eV	150-400	~4
2	May, 29, 1996	broken event, 2 hours	7-8.5	>50	n_e ~ 40-100 cm^{-3} $T_e \geq 5$ eV	80-110	45-60
2	April, 1, 1997	two events, <4 min each	8	40	n_e ~ 40-100 cm^{-3} $T_e \geq 5$ eV	80-110	~60
2	May, 11, 1997	single event, 3 hours 30 min	8-9	40-300	n_e ~ 40-100 cm^{-3} $T_e \geq 5$ eV	70-110	50-80
2	June, 22, 1997	broken event, 3 hours	~9	>75	n_e ~ 40-100 cm^{-3} $T_e \geq 5$ eV	90-110	~50
2	June, 27, 1997	three events, <2 min each	8.8	130	n_e ~ 40-100 cm^{-3} $T_e \geq 5$ eV	90-110	~50

where $\theta_0 \subset [0, \pi/2]$ is the half-angle of a resonance cone, inside which thermal waves can propagate (real K). Substituting the value of K_L given by (5) into (2), one finds generally that two wave packets might significantly contribute to the induced potential at large distances by constructive interference, and the apparent wavelength depends on the observation angle [*Kolesnokova and Béghin,* 1999a].

As we are concerned here with the instability conditions of Polar antennas, which involve only frequencies just below ω_p in the isotropic case, we look here at frequencies just below the upper hybrid resonance ω_t, which replaces now ω_p as a cut off for the electromagnetic X mode. In order to make a comparison with the isotropic case in the same conditions of plasma density, with a ratio $\Omega_p = 4$, we show in Figure 6 the plasma response in two directions of observation for $\Omega = 1.03$, which is now just below the upper hybrid ($\omega_t/\omega_p \simeq 1.0308$). Notice that we use the same characteristic length λ_D for distance normalization as in the isotropic case.

One can see that the real part of the potential

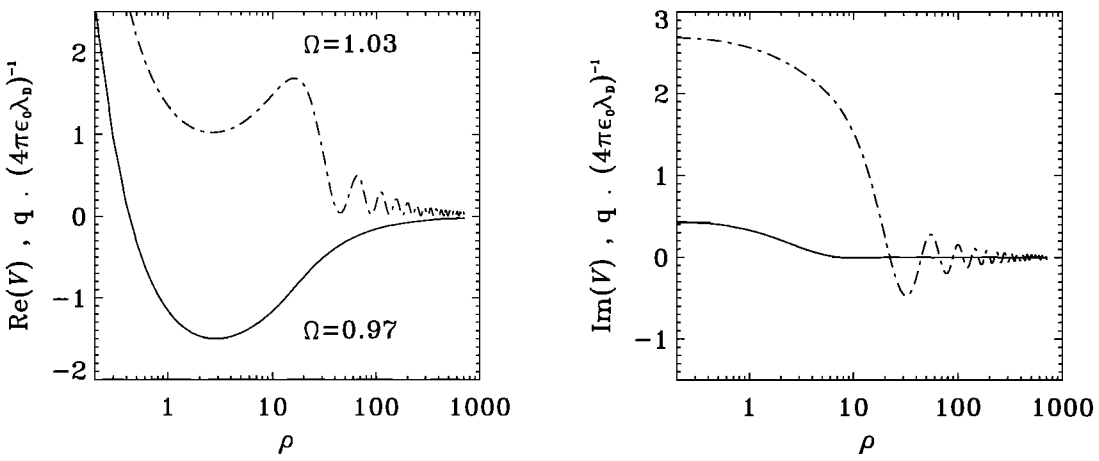

Figure 5. Real and imaginary parts of the potential versus the distance, induced by a pulsating point source in an isotropic Maxwellian plasma, at $\Omega = 1.03$ (dashed curves) and $\Omega = 0.97$ (solid curves). The Landau pole wavelength for $\Omega > 1$ is clearly visible at large distance.

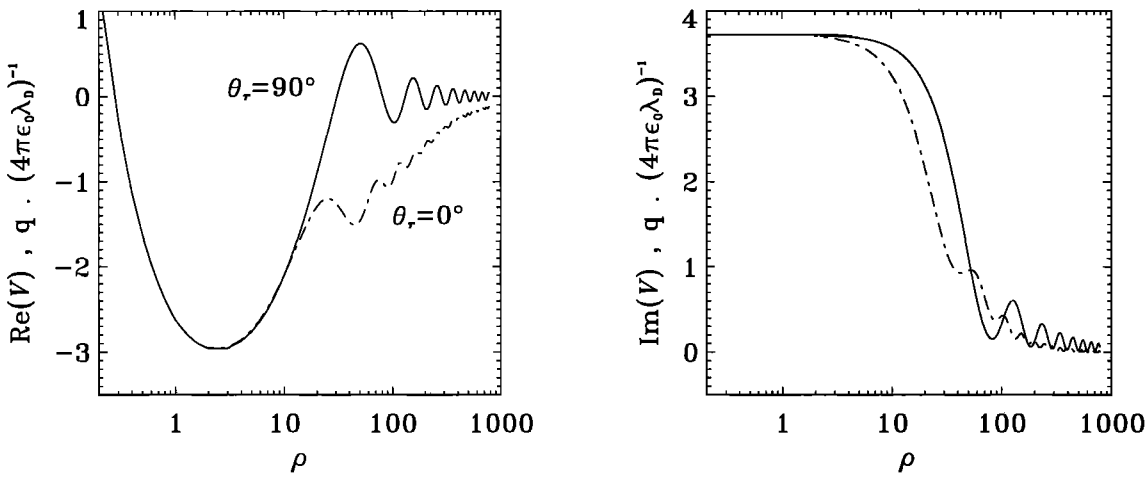

Figure 6. Same as Figure 6, but for $\Omega = 1.03$ just below the upper hybrid resonance when the Earth's magnetic field is taken into account with a ratio $\omega_p/\omega_c = 4$, and for both longitudinal and transverse directions of observation.

exhibits a sign shift similar to that of the isotropic case, whereas the frequency is lower than ω_p. Figure 6 also shows that the direction dependence appears only after about $4\lambda_D$, i.e., 1 Larmor radius since $\Omega_p = 4$. In summary, the presence of a weak magnetic field in the model would lead to a light shift in frequency, which satisfies the instability conditions, from below ω_p up to the upper hybrid range, while the anisotropy appears only for sizes larger than the Larmor radius.

3.3. Unmagnetized Streaming Plasma

We consider here a third possibility of plasma response, when the electron density is high enough to neglect the Earth's magnetic field, i.e., assuming $\Omega_p >> 10$, but when the plasma has a significant bulk velocity, of at least 10% compared to its thermal velocity. The plasma response to a pulsating point source can be obtained by computing the Laplace transform (LT) of the impulse response, as summarized here below. At the point source location, and at the time $t = 0$, we drive an impulse charge $q\,\delta(t)$, which induces at a distance r a time-varying potential $V(r, t)$. In a steady isotropic plasma this value is by definition the inverse Laplace transform of the plasma response as expressed by (3) in the Landau wave approximation. Using the LT tables [*Roberts and Kaufman*, 1976], one finds

$$V(r,t) = \frac{q}{4\pi\varepsilon_0\lambda_D}\frac{1}{\rho}\left[\delta(t) - \omega_p \sin\omega_p t\right] \quad t \le t_0,$$

$$V(r,t) = \frac{q}{4\pi\varepsilon_0\lambda_D}\frac{1}{\rho}\left[-t_0\omega_p^2 \int_t^\infty \frac{J_1(\omega_p\sqrt{u^2 - t_0^2})\sin\omega_p(u-t)\,du}{\sqrt{u^2 - t_0^2}}\right] \quad t > t_0, \tag{7}$$

$$t_0 = \frac{\rho}{\omega_p\sqrt{3}}\,.$$

It is easy to check that the first part of (7) is the cold plasma response, i.e., a permanent oscillation at the plasma frequency when ρ tends to infinity ($\lambda_D \to 0$). The second part is the thermal contribution, a damped oscillation at the same frequency. Once the impulse is emitted, the space distribution of the disturbance, as a function of time, is defined by (7) and no longer depends on the presence of the source. Moreover, if there is a relative move between the plasma and the two points under consideration, we are free to define the system of reference as the steady plasma with the observation point moving through it. The observation point, located at a given distance ρ_0 from the source, moves through the potential disturbance with the

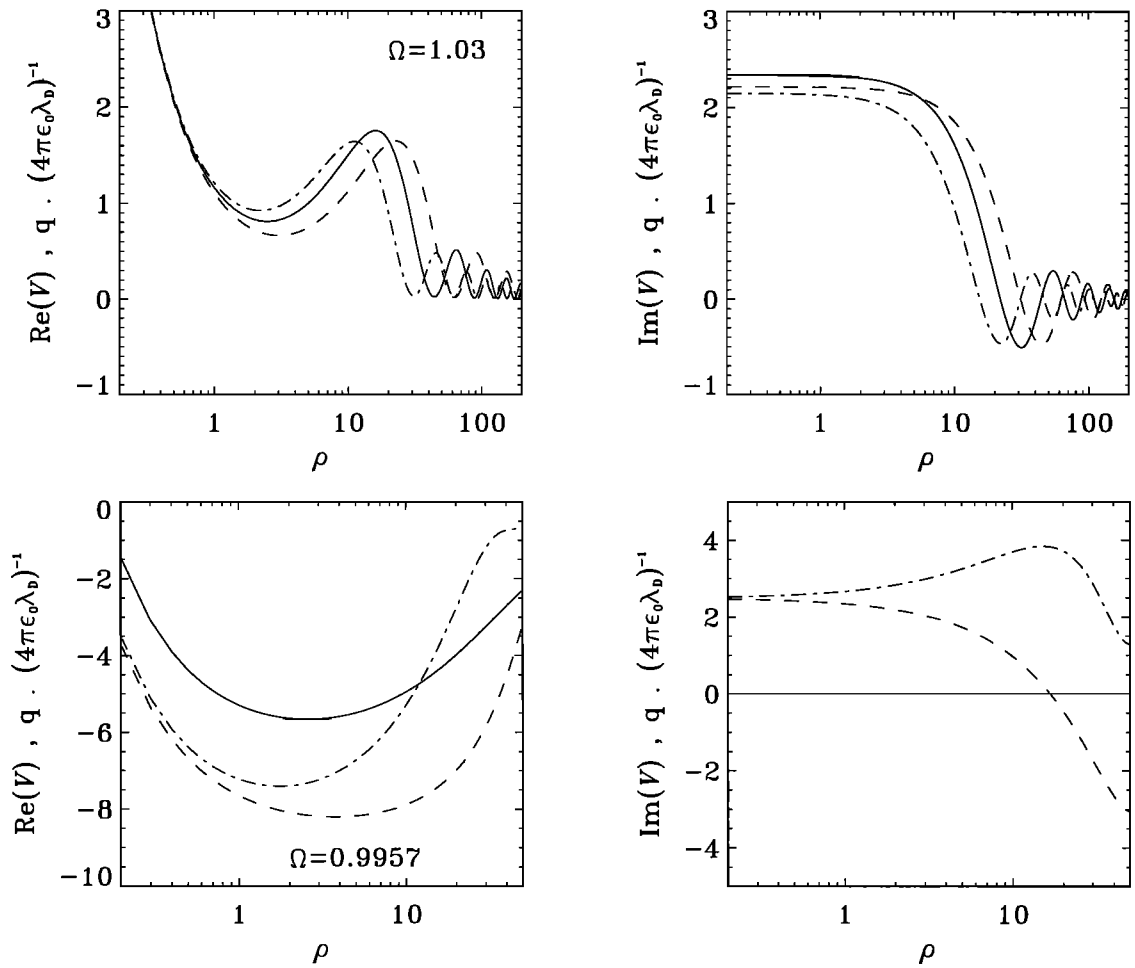

Figure 7. Comparison of the plasma responses above and below the plasma frequency between a streaming plasma (long-dashed and long-and-short-dashed curves) and a steady plasma (solid curves), using the Landau wave approximation. Long-and-short-dashed curves, backward motion, $\beta = 0.1$; long-dashed curves, forward motion, $\beta = -0.1$.

relative plasma drift velocity **V**, so that the distance becomes time dependent as

$$\rho = \left| \rho_0 + |\rho_0| \frac{t}{t_0} \beta \right| \ , \ \beta = \frac{\sqrt{2/3}}{v_t} \mathbf{V}, \qquad (8)$$

where v_t is the thermal velocity.

In the two-dimensional case, when the plasma is streaming in any direction with respect to the antennas, the evaluation of the impulse response along the antenna would be extremely complicated. We choose here to limit the present study to the parallel and anti-parallel conditions only, which is a sufficient analysis for understanding of the instability mechanism. Then, we consider β as a positive or negative value corresponding to backward or forward motion, respectively, of the plasma with respect to the vector ρ_0. From (7) and (8) it is clear that if $\beta > 1$, the thermal contribution will never be seen at the observation point. This is the simplest situation since the potential is given by the cold plasma contribution only, i.e., the LT of the first term in (7) by replacing ρ by $\rho_0 (1 + t\beta/t_0)$. However, we are considering here more realistic conditions with a relatively slow bulk velocity, such as $\beta < 1$. The computation is then much more complex since the thermal wave is seen some time after t_0 and the integral in (7) must be computed numerically, which will not be commented upon here since we have limited the discussion to the results applied to our problem of antenna instability only.

One of the more interesting differences between the plasma responses in a streaming plasma and those in a steady one lies below the plasma frequency (Figure 7). First, for the real part of the plasma response the negative part between 1 and 10 λ_D is much more pronounced than in a steady plasma, and second, a significant imaginary part appears, whereas it is absent in a steady hydrodynamic plasma. This results from a phase shift of the oscillation in the time response, which is obvious even in the cold plasma contribution of (7) when ρ is time dependent. The effect reduces to spread out the spectrum of the plasma response around the plasma resonance. For frequencies above the plasma resonance where a real Landau wave exists, there is an usual Doppler shift of that wave, as shown in Figure 7 and in agreement with the results obtained by using a different approach [*Michel*, 1976].

4. Instability Mechanism

4.1. Nyquist Criterion for Stability

Our approach consists of solving the transfer function of the equivalent circuit, sketched in Figure 2. We will use here the Nyquist's criterion approach, as previously applied to the study of the stability of antennas on the FR-1 satellite [*Fiala*, 1970]. We assume a given HF voltage V_0 at the output of the preamplifier, and we calculate the transfer function V_s/V_0 in open loop, in a wide frequency range around the plasma frequency. The unknown quantity is the sphere potential, which is induced by electrostatic coupling with the stubs through the plasma.

In the open-loop configuration the Nyquist transfer function is defined as

$$f(\omega) = A(\omega)\ V_s/V_0, \qquad (9)$$

where the preamplifier gain is a complex quantity defined as $A(\omega) = |A| \exp j\varphi$ (Figure 3).

Since we make use of dimensionless quantities such as the frequency Ω normalized to the plasma frequency ($\Omega = \omega/\omega_p$) and we know also that the plasma frequency can take any value in the range in which A varies significantly, the Nyquist diagram could be obtained only if the plasma frequency is fixed. Therefore, in order to remain in the general case, it is preferable to produce the Nyquist diagram versus the dimensionless frequency Ω, with the arbitrary value $A = 1$ for the gain of the preamplifier. Once the oscillation frequency is known, the actual preamplifier contribution can be taken into account to make the appropriate corrections in amplitude and phase. In the simplified analytic treatment we have assumed, as a first approximation, a direct link to the stub (C_s infinite), knowing that the complementary contribution due to the preamplifier response through the high-pass filter C_s R_s is negligible in the range of interest (~50-500 kHz), so that we have $V_b \simeq V_0$. The problem resumes to search for the conditions when the amplitude of the transfer function V_s/V_0 is at least equal to 1 for some value of Ω; therefore the instability Nyquist's point (1, 0) in the complex plane may possibly be included inside the contour of the complete function $f(\Omega)$ provided that the phase condition is satisfied.

4.2. Physical Mechanism and Conditions of Instability

In order to understand the physical mechanism of the instability we start by writing the basic equations for the simplest configuration, describing the balance between voltages and charges of the different surfaces, according to the SCD method.

In the analytic approach we use the following first-order approximations: (1) The sphere radius r (40 mm) is such that $r << \lambda_D$; (2) for each half part of the stub of length l and radius a (Figure 1) we have $a << \lambda_D$ and $l \geq \lambda_D$; (3) the surface charge distribution σ along the stub is uniform, such that $\sigma = Q_l/2\pi al$, where Q_l is the charge of each of the half stubs, which are assumed identical, and with $Q_l = Q_b/2$; (4) the preamplifier input capacitance C_{in} and the leakage capacitance C_b are neglected with respect to the sphere capacitance, so that the sphere is floating, and $Q_s = 0$; (5) the attenuation due to the high-pass filter made by C_s, R_s is neglected, in order that $V_b = V_0$; and (6) the current i_6 (Figure 2) flowing from the stub through the plasma, returning to the long boom and to the spacecraft (S/C) structure, is assumed here to be collected at a single point located near the S/C center, at a distance $L >> \lambda_D$ by the charge $-Q_b$.

Under these conditions the potential on half stub 1, for example the half stub on the right-hand side of Figure 1, near the interface with the sphere, using cylindrical coordinates and neglecting the edge effect, is given by

$$(4\pi\varepsilon_0\lambda_D)\ V_0 = a\sigma \int_{0}^{2\pi}\int_{=0}^{l} U(\Omega,\rho)\,d\theta\,dx + a\sigma \int_{0}^{2\pi}\int_{2r}^{l+2r} U(\Omega,\rho)\,d\theta\,dx - Q_b U(\Omega,L), \qquad (10)$$

where

$$\rho = \frac{\sqrt{x^2 + 4a^2 \sin^2(\theta/2)}}{\lambda_D},$$

and $U(\Omega, \rho)$ is the plasma response as defined in (3). A similar equation is written for the potential induced on the sphere. Since the sphere is assumed to be floating, with $r << \lambda_D << l$, we use the same usual approximation as in the free space, i.e., that the sphere takes the space potential at the center of the gap, as if it were absent. This reads

$$\begin{aligned}(4\pi\varepsilon_0\lambda_D)\, V_s = {} & a\sigma \int_0^{2\pi}\!\!\int_r^{l+r} U(\Omega,\rho)\, d\theta\, dx \\ & + a\sigma \int_0^{2\pi}\!\!\int_r^{l+r} U(\Omega,\rho)\, d\theta\, dx \; - \; Q_b U(\Omega, L).\end{aligned} \tag{11}$$

From section 3 we know that whatever the plasma conditions are, the real part of U always contains the free-space contribution with the term $1/\rho$, which dominates at short distances and leads to a real pole in the first integral of (10). It is obvious that the contribution of the other terms in the development of $U(\rho)$ such as given by (4) will be almost identical for each integral in (10) and (11). Then, the real part of $(V_s - V_0)$ is controlled only by the free-space contribution, which reads

$$\begin{aligned}\mathrm{Re}(V_s - V_0) = {} & \frac{\mathrm{Re}\, Q_b}{4\pi\varepsilon_0 l}\left[\int_{r'}^{l'+r'} \frac{d\rho}{\rho} - \frac{1}{2}\int_{2r'}^{l'+2r'} \frac{d\rho}{\rho}\right. \\ & \left. - \int_0^{2\pi}\!\!\int_{\approx 0}^{l} \frac{d\theta\, dx}{4\pi\rho\lambda_D}\right] = \frac{\mathrm{Re}\, Q_b}{4\pi\varepsilon_0 l}\,\alpha \\ & \alpha = \ln a\sqrt{\frac{2}{rl}}.\end{aligned} \tag{12}$$

Here and from now on we will make use of the dimensionless values l', r', and L' of l, r, and L, respectively, normalized with respect to λ_D. Notice that the last integral in (12) is well known as giving the free-space capacitance of a long cylinder, as

$$C = Q_l / V_0 = 2\pi\varepsilon_0 l / \ln l/a$$

We take V_0 real and positive as a phase reference, so that in order to satisfy the first condition of the Nyquist criterion for instability the above quantity Re $(V_s - V_0)$ must be positive. With the actual dimensions of Polar antennas, α is negative (α = -5.5), and then we get the first condition for instability

$$\mathrm{Re}(V_s - V_0) > 0 \;\Rightarrow\; \mathrm{Re}\, Q_b < 0. \tag{13}$$

In other words, this condition implies that the stub impedance must be inductive since the voltage and the charge are out of phase. This condition excludes any instability in free space where the stub is a pure capacitance. From both real and imaginary parts of (10) and (11), using the phase reference condition $\mathrm{Im}\, V_0 = 0$ and $V_0 > 0$, we obtain

$$\begin{aligned}& (4\pi\varepsilon_0\lambda_D)\, V_0 = \mathrm{Re}\, Q_b \,\frac{X^2 + Y^2}{X}, \\ & \mathrm{Im}\, V_0 = 0,\ \mathrm{Re}\, Q_b < 0,\ \text{and}\ V_0 > 0 \Rightarrow X < 0; \\ & (4\pi\varepsilon_0\lambda_D)\,\mathrm{Re}\, V_s = \mathrm{Re}\, Q_b \,\frac{X^2 + Y^2 + \alpha X/l'}{X}, \\ & (4\pi\varepsilon_0\lambda_D)\,\mathrm{Im}\, V_s = -\mathrm{Re}\, Q_b \,\frac{\alpha Y}{X l'}; \\ & X = \frac{1}{4\pi l'}\left[\int_0^{2\pi}\!\!\int_{\approx 0}^{l'} \mathrm{Re}\, U(\rho)\, d\theta\, d\rho\right. \\ & \qquad \left. + \int_0^{2\pi}\!\!\int_{2r'}^{l'+2r'} \mathrm{Re}\, U(\rho)\, d\theta\, d\rho\right] - \mathrm{Re}\, U(L'), \\ & Y = \frac{1}{4\pi l'}\left[\int_0^{2\pi}\!\!\int_{\approx 0}^{l'} \mathrm{Im}\, U(\rho)\, d\theta\, d\rho\right. \\ & \qquad \left. + \int_0^{2\pi}\!\!\int_{2r'}^{l'+2r'} \mathrm{Im}\, U(\rho)\, d\theta\, d\rho\right] - \mathrm{Im}\, U(L').\end{aligned} \tag{14}$$

From the first condition (13) and from the above expression of V_0 we have deduced that X must be negative, which is achieved, according to the definition of X in (14), from the balance between the real parts of the plasma response coming from the charges distributed on the stub itself and from the return charges located on the S/C structure at the distance L'. Looking at the plot of Re U in Figure 5, we see immediately that such a condition cannot be satisfied for Ω = 1.03 whatever the value of the Debye length. This remains true for any frequency above the plasma frequency. On the contrary, it is easy to anticipate the condition to be satisfied for Ω = 0.97 due to the sign shift around $\rho \sim 0.4$. If the Debye length is such that $L' >> 10$, the contribution of return charges can be neglected, and if the negative branch of

the curve involves a significant part of the stub, the integration could lead to a negative value for X.

This is basically the physical mechanism for the Polar antennas instability, which can occur only when the impedance of the stub becomes inductive. This is generally known to be the case for dipole antennas below the plasma frequency, in isotropic plasma, and when the dipole size is longer than ~10 Debye lengths. However, another condition must be satisfied here regarding the Nyquist criterion, due to the phase response of the preamplifier, which will be introduced now as a second constraint.

Since the preamplifier has a negative phase response (Figure 3), the transfer function V_s/V_0 must have exactly the opposite value at the Nyquist point. Then, from (14), and knowing that α and X are negative, we obtain the second condition for instability

$$\tan(\varphi) = \frac{\mathrm{Im}\, V_s}{\mathrm{Re}\, V_s} = -\frac{\alpha Y}{\alpha X + l'(X^2+Y^2)} > 0, \quad (15)$$

thus, $Y > 0$. The immediate consequence of this constraint is that the instability below the plasma frequency cannot be explained by using the purely hydrodynamic approach for the plasma, since $Y = 0$. However, in isotropic Maxwellian plasmas the kinetic contribution (Figure 5) is large enough to satisfy (15) under certain conditions. The solution of (15) for the antennas E_u and E_v is plotted in Figure 8 for $\varphi = 8°$ and two values of λ_D (50 cm and 2 m) corresponding to $l' = 6$ and 1.5 respectively.

Let us consider now the development of Re U as given by (4) for $\Omega < 1$. Using (14), we get

$$X = \frac{\ln\left(\frac{l^{3/2}}{a\sqrt{2r}}\right)}{l'} - \frac{1}{\sqrt{3|\varepsilon_c|}} + \frac{l'}{12} + \frac{1}{L'|\varepsilon_c|}, \quad \varepsilon_c < 0. \quad (16)$$

For $\Omega = 0.97$, i.e., $\varepsilon_c = -6.28 \times 10^{-2}$ corresponding to the example plotted in Figure 5, with $\lambda_D = 50$ cm, we obtain $X \approx -0.03$, which could marginally satisfy the first instability condition. Therefore, for the imaginary part of U, we take the contribution of the electrokinetic mode, as derived from the plot given in Figure 5, i.e., $Y \approx 0.5$. From (15) we get $\varphi \approx +59°$, which also satisfies theoretically the second condition. However, such a large phase shift can compensate the preamplifier's response only at frequencies of oscillation of ~500 kHz (Figure 3), i.e., with an

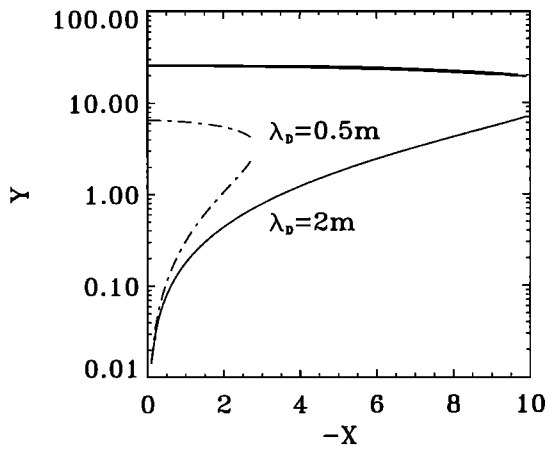

Figure 8. Relation between X and Y for the antennas E_u and E_v allowing the phase condition at the Nyquist point for two different values of Debye length, and $\varphi = 8°$ to be satisfied.

electron density of the order of 3000 cm^{-3}. With $\lambda_D = 50$ cm this leads to an electron temperature of 14 eV, which could be acceptable in regions of type-2 instabilities, but there, the oscillations never exceed 110 kHz, and an electron density of 3000 cm^{-3} seems to be a totally unrealistic value in these regions.

Let us consider now a more realistic phase shift of ~8°, corresponding to an average value of oscillations lying around 100 kHz (120 cm^{-3}). We keep the same value of $Y \approx 0.5$, which remains almost constant as long as $\Omega < 1$. Taking again $\lambda_D = 50$ cm, we get $T_e \sim 0.6$ eV, which is now a reasonable value in the dense plasmasphere where type-1 oscillations are observed. From Figure 8 we obtain the new instability point ($Y \approx 0.5$; $X \approx -1$). By substituting the values of X and l' in (16) we get $\varepsilon_c = -2.8 \times 10^{-2}$, i.e., an oscillation frequency $\Omega \approx 0.986$, which is, in fact, very close to the above value (0.97). This proves that the Nyquist contour is very sensitive around the plasma frequency, as confirmed by the numerical modeling.

From this simplified analytic approach we understand quite well the instability mechanism, which requires the general conditions given by (13)-(15), whatever the plasma model could be. In the simplest case of an isotropic Maxwellian plasma we have found that a Debye length of 50 cm satisfies the instability conditions for both E_u and E_v antennas. Such a simplified approach does not allow a detailed evaluation, because of the initial approximations made. The real charge distributions on all surfaces, the finite value of the preamplifier input capacitance, and

the precise evaluation of the plasma response are anticipated to produce more complex constraints, whose evaluation is the purpose of the numerical modeling. However, we will come back to the analytic evaluation in section 6.

5. Numerical Modeling

A simulation code has been developed, based on the SCD method proposed by *Béghin and Kolesnikova* [1998], producing the sphere-stub transfer function V_s/V_0 for the antenna E_u, as a function of frequency and Debye length. We have used the finite element method, which involves division of all surfaces into discrete elements (including wire booms and spacecraft body when necessary), to determine the currents i_3 and i_6 flowing from the sphere and the stubs, respectively, into the plasma. Independently from the general equations of the SCD method describing the electrostatic equilibrium of each surface element in contact with the plasma, we use the following particular interconnection equations obtained here from the equivalent scheme in Figure 2:

$$V_0 C_b - V_s(C_b + C_{in}) = -j\frac{i_3}{\omega} = Q_s, \qquad (17a)$$

$$C_s(V_0 - V_b) + j\frac{V_b}{\omega R_s} = -j\frac{i_6}{\omega} = Q_b, \qquad (17b)$$

where i_3 and i_6 are the currents flowing from the sphere and the stub surfaces through the plasma, Q_s and Q_b are the total charges accumulated at the sphere and stub surfaces, and C_{in} is the input capacitance of the preamplifier.

According to the available information [*Harvey et al.*, 1995; L. Åhlen, Swedish Institute of Space Physics, private communication,1997] we have used the following standard values for the passive parts:

$$C_{in} = 2 \text{ pF}, C_b = 2 \text{ pF}, C_s = 220 \text{ nF}, R_s = 100 \text{ k}\Omega.$$

Those values may be subject to a quite inaccurate determination, but since they introduce a second-order effect, this inaccuracy has been found to have no significant consequence on the results. In all cases, we assume that both the boom and sphere cross sections are much smaller than the Debye length, so that we can use the mesh structure approximation [*Béghin and Kolesnikova,* 1998]. Consequently, we ignore the presence of a weak ion sheath around the antenna. The charge distributions on the wire boom (subcrcipt *L)*, the spacecraft body (subscript S/C), the sphere (subscript *s*), and the stub (subscript *b*) must also satisfy the following boundary conditions on every surface, i.e., in the simple case of a purely symmetric dipole:

$$V_L = V_{S/C} = 0 \ , \ V_s = \text{const} \ , \ V_b = \text{const}. \qquad (18)$$

In the electrostatic approximation and for mesh-like structures the potential of each surface element is the sum of the contributions induced through the plasma by all charge elements contained in the system. Then, the SCD method consists of a solution of a linear system involving all unknown surface charge elements, by applying the plasma response function to each of them and by closing the system with (17a), (17b), and (18).

The previous analytic analysis has shown that the hydrodynamic thermal waves in isotropic plasma create the conditions for instability at frequencies below the plasma frequency and for certain values of Debye length, which are determined essentially by the length of the stub. This is confirmed by the code.

For $\lambda_D = 50$ cm the code predicts that the modulus of V_s / V_0 is marginally smaller than 1 (Figure 9), thus the antennas are stable at any frequency, independent

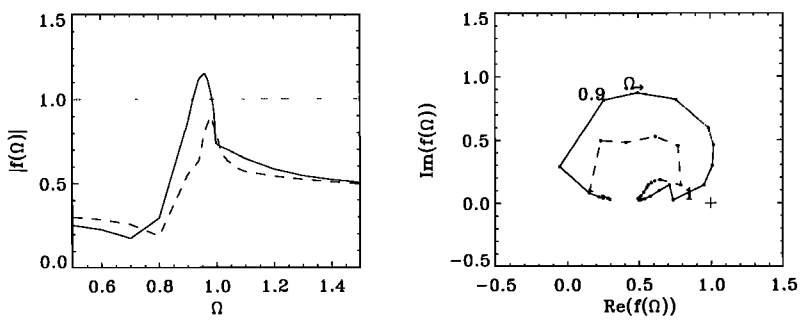

Figure 9. (left) Amplitude of the transfer function and (right) Nyquist's diagram for the dipole E_u, with a perfect preamplifier ($A = 1$), for $\lambda_D = 50$ cm (dashed curves) and $\lambda_D = 30$ cm (solid curves).

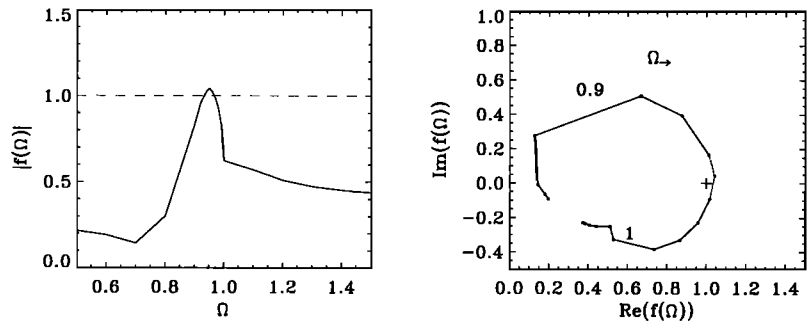

Figure 10. Same as Figure 9, but including the actual transfer function of the preamplifier and the actual stub feeding through the stray capacitance C_s, for the antenna E_u, with f_p = 200 kHz and λ_D = 28 cm (n_e = 500 cm^{-3} and T_e = 0.7 eV).

of the preamplifier response. For shorter values, say λ_D = 30 cm, the modulus oversteps the critical value of 1 in a small frequency range below Ω = 1. One can see in Figure 9 however, that the Nyquist instability point (1, 0) lies outside the contour when we consider a perfect preamplifier (A = 1). However, since the preamplifier response has a negative phase shift of ~10°-20° in the usual range of oscillations, it will be enough to rotate the contour toward the instability point. According to Figure 3, if the plasma frequency lies around 200 kHz, such a condition is satisfied and the antenna will oscillate for λ_D = 28 cm (Figure 10), i.e., for T_e ~ 5200 K (0.7 eV) and n_e ~ 500 cm^{-3}, which confirms the first-order values obtained with the analytic estimation.

One of the main differences between the numerical code and the analytic estimation concerns the charges distributed on the spheres, neglected in the analytic approach, and the distribution of return charges along the booms [*Kolesnikova and Béghin*, 1999b]. Large-amplitude surface waves are lying along the long booms in the worst case, when all return currents are supposed to be purely symmetrical, i.e., assuming a perfect balance between opposite charges distributed symmetrically on each half dipole and a quasi-point S/C surface. This is an unrealistic ideal case because the oscillations of independent spheres have no reason to be correlated. Therefore most of the return charges in reality should be distributed at the S/C surface, reducing accordingly the contribution of the surface wave charges along the booms. Thus the real situation would be reduced to an equivalent return current located somewhere on the boom close to the S/C center, as assumed in the analytic treatment.

When the antenna oscillates near a given value of the plasma frequency, we are able to define a lower limit for the Debye length at this time, i.e., an upper limit for T_e. The immediate consequence of this effect is a different threshold of λ_D for each antenna. If we take into account the preamplifier response, we are then able to plot the variations of this threshold in terms of the electron temperature T_e versus the plasma frequency for both antennas (E_u and E_z) of different lengths. This is shown in Figure 11.

The data analysis of bias current of different spheres and of spacecraft potential over 1 year [*Escoubet et al.*, 1997] reveals that the E_z antenna probably never oscillates. Thus, from the result given by Figure 11, we could deduce that the plasma parameters f_p and T_e (which allow the oscillations in quasi-unmagnetized plasma) are lying between the two curves. Considering the case of type-1 instabilities occurring in the dense plasmasphere at low L shell, the range of the

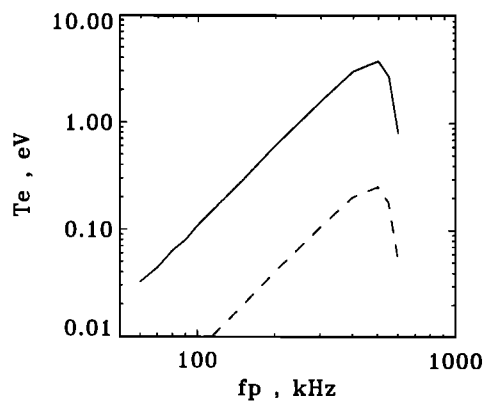

Figure 11. Variation of the instability threshold (T_e, f_p) for the antennas E_u (solid curve) and E_z (dashed curve) in an unmagnetized thermal plasma. For each antenna the region above the curve is stable, and the region below is unstable.

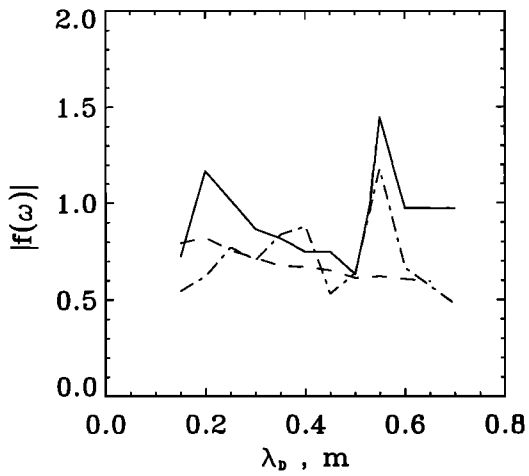

Figure 12. Modulus of the transfer function in the vicinity of Ω_t (1.03), for two different orientations of the antenna with respect to $\mathbf{B}_0$: 0° (solid curve) and 90° (long-and-short-dashed curve), with $\Omega_p = 4$ and $A = 1$. For reference the result for isotropic model is plotted with a long-dashed curve.

oscillation frequency (150-400 kHz as given in Table 1), i.e., $n_e \sim$ 100-2000 cm^{-3}, and the range of $T_e \sim$ 0.3-2 eV, which are both of them bounded by our model (Figure 11), are perfectly compatible with standard estimations and previous measurements in this region [e.g., *Décréau et al.*, 1978].

We have checked that the values of capacitances in the equivalent circuit given in Figure 2 are not critical, so that variations of a factor of 2 around their nominal value do not significantly change the final result. In particular, the value of $C_s = 220$ nF leads to practically the same result as a short circuit ($V_b = V_0$).

In order to interpret the modulation of oscillations as a function of the dipole's orientation with respect to the Earth's magnetic field, as shown in Figure 4, we have used in our code the plasma response corresponding to the model described in section 3.2, for two orientations only, i.e., parallel and perpendicular.

In a typical weakly magnetized plasma where type-1 oscillations are observed ($\omega_p/\omega_c = 4$), the results show that the conditions for instability are slightly changed, as expected from the behavior of the plasma response plotted in Figure 6. The first remark is that the conditions of instability are satisfied in the upper hybrid range, above the plasma frequency instead of below as in the isotropic case. This is explained by the analytic treatment as being due to the sign shift of the real part of the plasma response in this range (Figure 6).

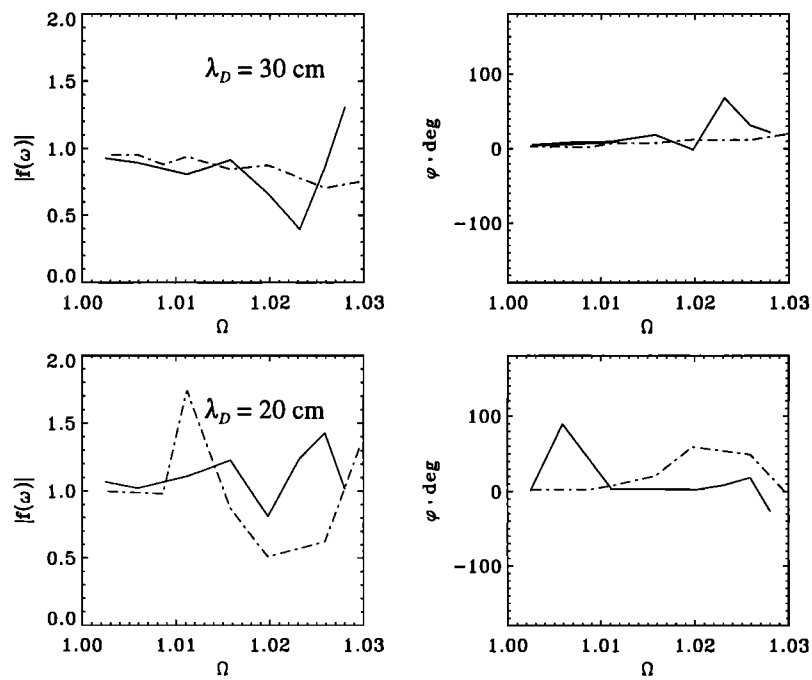

Figure 13. Modulus and phase of the transfer function in the upper hybrid range, for two different values of λ_D, $\Omega_p = 4$, $\Omega_t = 1.0308$, and $A = 1$. The dipole angle with respect to $\mathbf{B}_0$ is 0° (solid curve) or 90° (long-and-short-dashed curve).

Table 2. Summary of Measured and Predicted Ranges of Parameters for Each Type of Instability

Type	f_t (Fundamental) ~ f_p, kHz	R_E	L	f/f_{ce}	n_{e_3} cm^{-3}	Probable T_e, eV	Probable Bulk Velocity in the Plane u,v, km s^{-1}
1	$150 \le f \le 400$	2-4	≤4	≥3.5	300-2000	~1	~0
2	$70 \le f \le 110$	≥7	≥40	≥50	60-150	4-12	140-250

By comparing the values of the transfer function, for the two orientations of the antenna shown in Figure 12, we conclude that just below the upper hybrid frequency ($\Omega_t = 1.0308$) the most favorable conditions for instability occur when the antenna is aligned with the magnetic field, which is in agreement with the observations when the oscillations are just vanishing (last part of sequence in Figure 4). More precisely, the variations of the transfer function versus the frequencies in the upper hybrid range (Figure 13) show that the instability can be triggered for $\lambda_D = 30$ cm, at frequencies just below Ω_t and only in the parallel direction with respect to the magnetic field. If we refer to the case shown in Figure 4 around 1203 SCET, the deduced plasma parameters in this case can be estimated as $f_p \approx 215$ kHz, $n_e \approx 570$ cm^{-3}, and $T_e \approx 0.9$ eV.

However, for shorter Debye length ($\lambda_D = 20$ cm) there are two possible frequencies of oscillation, namely, $\Omega \approx 1.012$ and 1.026 (Figure 13), corresponding to the antenna orientations perpendicular and aligned to the magnetic field, respectively. During the spin period the oscillation frequency is predicted to be modulated between these two values. Such a phenomenon is clearly visible in the period between 1200:20 and 1200:50 SCET in Figure 4. With now $\lambda_D = 20$ cm instead of 30 cm, and $f_p \approx 225$ kHz, i.e., $n_e \approx 625$ cm^{-3}, we have $T_e \approx 0.45$ eV, which could reveal an important gradient of temperature in the boundary region of the plasmapause, where the type-1 oscillations suddenly vanish.

If such plasma parameters, deduced from the simulation, are compatible with the expected values in the region where type-1 oscillations occur, they are unlikely to exist in the outer cusp region during high-density events, where warmer temperatures are expected (Table 1). Here, a more complex plasma model as discussed in section 3.3 is needed to account for the observations. Unfortunately the existing numerical code cannot be easily applied to this plasma model. Therefore we will use the analytic approach to explain the type-2 instabilities.

6. Type-2 Instabilities

For the case study shown in Plate 1, on May 11, 1997, around 1200 SCET, there is some indication that during this event the Polar spacecraft was crossing a high-density suprathermal electron cloud of several eV, probably in the turbulent boundary layer located just outside the magnetopause current layer in the cusp (J. Pickett, private communication, 1997). If we assume a steady plasma, such a thermal energy leads to a Debye length of the order of at least 1-2 m as a threshold value for instability, which is excluded according to the results given in section 5. These facts suggest that such a plasma cannot be assumed to be isotropic and steady with respect to the spacecraft.

Returning to the analytic approach, we must first predict some limit of its validity. The estimation of the normalized inductance of the stub ($-X$) in (16) is valid as long as the return charges are located at large normalized distance L', so that their contribution is that of the cold plasma only ($1/L' \mid \varepsilon_c \mid$). To be valid, the thermal contribution term with the exponential in (3) must be negligible; thus $L' (\mid \varepsilon_c \mid /3)^{1/2} > 1$. If we consider now a Debye length of the order of 2 m, which could be a reasonable value in the region concerned, we find an upper limit of the instability frequency such as $\mid \varepsilon_c \mid > 3 \times 10^{-3}$ in order that (16) be valid. Let us take, for instance, $\mid \varepsilon_c \mid = 8.25 \times 10^{-3}$, which reduces the contribution of the return charges to less than 20% of that of the stub. From (16) we get $X = +4.35$, a value which is well out of range of the first condition for instability and which confirms the fact that the largest theoretical Debye length leading to instability of the antennas E_u or E_v in a steady Maxwellian plasma is less than 50 cm. Independently of geophysical considerations, this result confirms that the steady plasma model cannot explain the type-2 oscillations.

Let us consider now a streaming plasma as in section 3.3, with a ratio of the order of 12% between the drift and the thermal velocities ($|\beta| = 0.1$). Still at the same frequency as above ($|\varepsilon_c| = 8.25 \times 10^{-3}$, i.e., $\Omega = 0.9957$), we can deduce from Figure 7 the first-order values of Re U and Im U for $\lambda_D = 2$ m, $l' = 1.5$, $L' = 32.5$ and $\beta = +0.1$, i.e., when the plasma flow is directed from one of the sensors toward the S/C structure, which reads

$$\begin{aligned} &\mathrm{Re}\,U(l') \approx 1/l' - 8.3,\ \mathrm{Im}\,U(l') \approx 2.6,\ l' < 2 \\ &\mathrm{Re}\,U(L') = -0.8,\ \mathrm{Im}\,U(L') = 2.42,\ L' = 32.5. \end{aligned} \tag{19}$$

Then, from (14), and performing a similar integration as for (16), we obtain $X = -0.95$ and $Y = 0.18$, which is exactly the instability point for $\lambda_D = 2$ m with a phase shift of 8°, such as can be checked in Figure 8. In the opposite direction ($\beta = -0.1$, Re U (L') ≈ - 5.5), we obtain $X = +3.75$ which is a stable point. Thus the instability vanishes somewhere between those two directions.

This result proves that each sensor of the E_u or E_v antennas can reach the instability regime at least once per spin period when it is in front of an electron flow of 60-150 cm^{-3} density ($70 < f_p < 110$ kHz), 4.5-11 eV temperature ($\lambda_D = 2$ m), and 140-250 km s^{-1} bulk velocity ($\beta = 0.1$, i.e., 0.07-0.17 eV). It seems, indeed, that the high-time-resolution data analysis of the dc bias of spheres during the type-2 oscillations reveals one spin period symmetry instead of one-half period as for type 1, with a shift of 180° between the two opposite sensors of the same dipole (R. Grard, Space Science Division, European Space Agency, private communication, 1998).

A three-dimensional data analysis would allow us to check our theoretical model and to use this fact for a measurement of the electron bulk velocity, both in amplitude and in direction. We could have certainly found other values of the above plasma parameters within a probable window able to satisfy the type-2 instability conditions, but this is beyond the purpose of the present study and would require the development of a new numerical code. At the same time, it would be necessary to make a comparison of the parameters predicted by our model with data obtained by other experiments on board.

7. Summary and Conclusion

The investigation of Polar's antenna instability based on the general SCD method has allowed us to understand the involved physical mechanism after a theoretical and simplified analytical study, confirmed as far as possible by a numerical code. The critical plasma parameters which are necessary to trigger the instabilities have been identified, and their predicted values from the modeling are found to be reasonable with respect to geophysical considerations. The main results are as follows: (1) The instability can be triggered only when the impedance of the guard-stub with respect to the reference structure is inductive, which depends essentially on the frequency compared to the plasma frequency and on the bulk and the thermal electron velocity distributions. (2) The instability is most likely to be triggered always in the range of frequencies from ~ $0.9 f_p$ to ~f_t for the plasma conditions encountered along Polar's spacecraft orbit. (3) The instability conditions involve the full transfer function of the preamplifier, including the phase response which strongly constrains the plasma parameters. (4) In a quasi-Maxwellian plasma the occurrence of the type-1 instability for the long antennas (E_u-E_v), while at the same time the short one (E_z) remains stable, leads to a range of Debye lengths lying between 10 and ~30 cm in the concerned regions. The upper limit of oscillations (~400 kHz) due to the preamplifier cutoff leads to a maximum electron density of ~2000 cm^{-3} for type-1 oscillations and, consequently, to a temperature range of 0.3-3 eV. (5) In a streaming plasma the upper limit of the Debye length for triggering the type-2 instability can increase up to about the size of the guard-stub (~2 m), depending on the ratio between the bulk and thermal velocities. (6) The frequency and the strength of the oscillations are attitude dependent with respect to the Earth's magnetic field orientation, leading to a simultaneous half-spin period modulation for each sensor of every dipole antenna in the case of the type-1 instabilities. (7) For type-2 instabilities the spin modulation is predicted to be dominated by the direction of the plasma bulk velocity with respect to the spacecraft orientation, leading to one spin period modulation and 180° phase shift between the sensors of the same dipole, with the strongest oscillation occurring when the angle between the sensor-spacecraft line and the bulk velocity is a minimum.The model-predicted plasma parameters (n_e, T_e, and bulk velocity) which are favored to trigger the two different types of oscillations are summarized in Table 2, together with the local geophysical parameters (R_e, L, and f_{ce}).

Further investigation will be necessary to improve our modeling and to compare the above-predicted plasma parameters to the available onboard

measurements. A positive return from the troubling phenomenon of this instability would be to make use of it for geophysical diagnostic purposes every time the instabilities occur.

Acknowledgments. The authors are grateful to F. Mozer from Berkeley University, D. Gurnett and J. Pickett from Iowa University, R. Grard from ESTEC, and L. Åhlen from IRF-U for providing them with invaluable information about the Polar wave experiments, and they greatly appreciated several stimulating and fruitful discussions with those persons and their teams. One of the authors (E.K.) is grateful to LPCE from the Centre de la Recherche Scientifique, the Solar System Division from ESA and the Radio and Space Plasma Physics Group from University of Leicester, for providing her with grants and facilities during this study. The authors thank Emma Bunce for the checking and corrections of the manuscript.

References

Béghin, C., Series expansion of electrostatic potential radiated by a point source in isotropic Maxwellian plasma, *Radio Sci., 30*, 307-322, 1995.

Béghin, C., and E. Kolesnikova, Theory and applications of the discrete surface-charge distributions for modelling of electric antennas in isotropic kinetic plasma, *Rep. LPCE/NTS/045.B,* Lab. Phys. Chim. Environn., Cent. Nat. de la Rech. Sci., Orléans, France, 1997.

Béghin, C., and E. Kolesnikova, The surface-charge distribution approach for modelization of quasi-static electric antennas in isotropic thermal plasma, *Radio Sci., 33,* 503-516, 1998.

Décréau, P. M. E., C. Béghin, and M. Parrot, Electron density and temperature, as measured by the mutual impedance experiment on board GEOS-1, *Space Sci. Rev., 22,* 581-595, 1978.

Escoubet, C. P., R. Grard, B. Jacobsen, and R. Schmidt, Polar oscillation characteristics, internal report Space Sci. Div., Eur. Space Res. and Tecnol. Cent., Eur. Space Agency, 1997.

Fiala, V., Stabilité des antennes électriques du satellite FR1 dans le plasma ionosphérique, *Ann. Télécommun., 25,* 259-264, 1970.

Gurnett, D. A., et al.,., The Polar Plasma Wave Instrument, *Space Sci. Rev., 71,* 597-622, 1995.

Harvey, P., et al., The Electric Field Instrument on the Polar satellite, *Space Sci. Rev., 71,* 583-596, 1995.

Kolesnikova, E., and C. Béghin, Potential around an oscillating point-charge in a weakly magnetized plasma, *Rep. LPCE/NTS/063.B*, Lab. Phys. Chim. Environn., Cent. Nat. de la Rech. Sci., Orléans, France, 1999a.

Kolesnikova, E., and C. Béghin, The instability problem of the electric antennas of the Polar and Cluster-1 types near the plasma resonances, *Rep. LPCE/NTS/065.B*, Lab. Phys. Chim. Environn., Cent. Nat. de la Rech. Sci., Orléans, France, 1999b.

Michel, E., Analytical derivation of the HF electrostatic potential created by an oscillating point source in a streaming water-bag plasma, *J. Plasma Phys., 15*, 395, 408, 1976.

Quemada, D., *Ondes dans les Plasmas*, Hermann, Paris, 1968.

Roberts, G. E., and H. Kaufman, *Table of Laplace Transforms,* W. B. Saunders, Philadelphia, Pa., 1976.

Spitzer, L., *Physics of Fully Ionized Gases,* 2nd ed., Wiley-Interscience, New York, 1962.

C. Béghin, Laboratoire de Physique et Chimie de l'Environnement, Centre National de la Recherche Scientifique, 45071 Orléans Cedex 2, France. (cbeghin@cnrs-orleans.fr)

E. Kolesnikova, Department of Physics & Astronomy, University of Leicester, University Road, Leicester LE1 7RH, England, U. K. (elka@ion.le.ac.uk)

(Received December 8, 1999; revised June 5, 2000; accepted August 29, 2000.)